I. GLOBAL PROPERTIES OF THE PHOTOSPHERE

https://doi.org/10.1017/S0074180900043941 Published online by Cambridge University Press

MODELS OF THE SOLAR PHOTOSPHERE

EUGENE H. AVRETT
Harvard-Smithsonian Center for Astrophysics
60 Garden Street
Cambridge, Massachusetts 02138, USA

ABSTRACT. This review summarizes the main properties of the available theoretical models of the solar photosphere and the semiempirical models based primarily on observed spectra in different wavelength regions. LTE and non-LTE semiempirical models are compared with LTE and non-LTE theoretical (radiative equilibrium) models calculated with and without convective energy transport. Atomic and molecular lines throughout the spectrum affect the model calculations in essential ways. The temperature-minimum region, considered as the upper boundary of the photosphere, is discussed in detail, in view of the substantial non-radiative cooling in this region. Results are shown to illustrate the relationship between average one-dimensional models and Nordlund's three-dimensional convection models.

1. Introduction

One of the principal ways of learning how the solar atmosphere varies as a function of depth is to observe the Sun at different wavelengths, since variations of the opacity with wavelength correspond to a change of the depth at which the emerging radiation is formed. Opacity variations with wavelength occur between different regions of the spectrum, and within spectral lines.

The variation of atmospheric parameters also can be studied by means of center-to-limb observations, since the intensity at a given wavelength seen near the limb emerges from a higher level in the atmosphere than that seen near disk center. As discussed by Nelson (1978), other observational constraints on models of the atmosphere are the brightness variations and motions observed in solar granulation.

The present review will deal principally with models determined from observed spectra at different wavelengths, since the widest range of depths can be studied in this way.

2. The Solar Spectrum

Figure 1 is a sketch of the observed brightness temperature T_b of the Sun as a function of wavelength between 1 cm and 10 nm. The lower panel indicates the principal sources of opacity at the depths where the observed radiation is formed. Here $T_b(\lambda)$, is the temperature of an isothermal atmosphere in LTE without scattering that gives the same central intensity (or flux from the entire disk) as is observed.

The observed radiation is emitted from the greatest depth in the atmosphere at 1.6 μm where the opacity has a minimum. At this wavelength the central brightness temperature is about 6800 K. The brightness temperature of the disk is about 500 K lower because of limb darkening.

J. O. Stenflo (ed.), Solar Photosphere: Structure, Convection, and Magnetic Fields, 3–22.

For $\lambda > 1.6$ μm the opacity becomes larger as λ increases, unit optical depth occurs higher in the atmosphere, and T_b decreases, reaching a minimum value of about 4500 K at 150 μm. Here there is little center-to-limb variation and the disk and central brightness temperatures are the same (apart from the presence of active regions at various locations on the disk that are brighter than the average quiet Sun). The increase of T_b for $\lambda > 150$ μm (where the opacity continues to increase) is due to the increase of temperature in the chromosphere.

For $\lambda < 1.6$ μm the opacity also becomes larger as λ decreases, and T_b decreases to a minimum value of about 4400 K near 160 nm. The subsequent increase of T_b in the region $\lambda < 160$ nm again is due to the chromosphere rise in temperature. We will discuss only the photosphere in this review, from the deepest observable layers to the temperature minimum region.

Figure 2 shows the observed flux from the entire disk between 2 μm and 250 nm, and the corresponding disk brightness temperature. The maximum in T_b at 1.6 μm corresponds to only a slight inflection in the flux distribution at this wavelength. These are broad-band flux measurements that do not distinguish between regions having a well defined continuum and regions dominated by absorption lines.

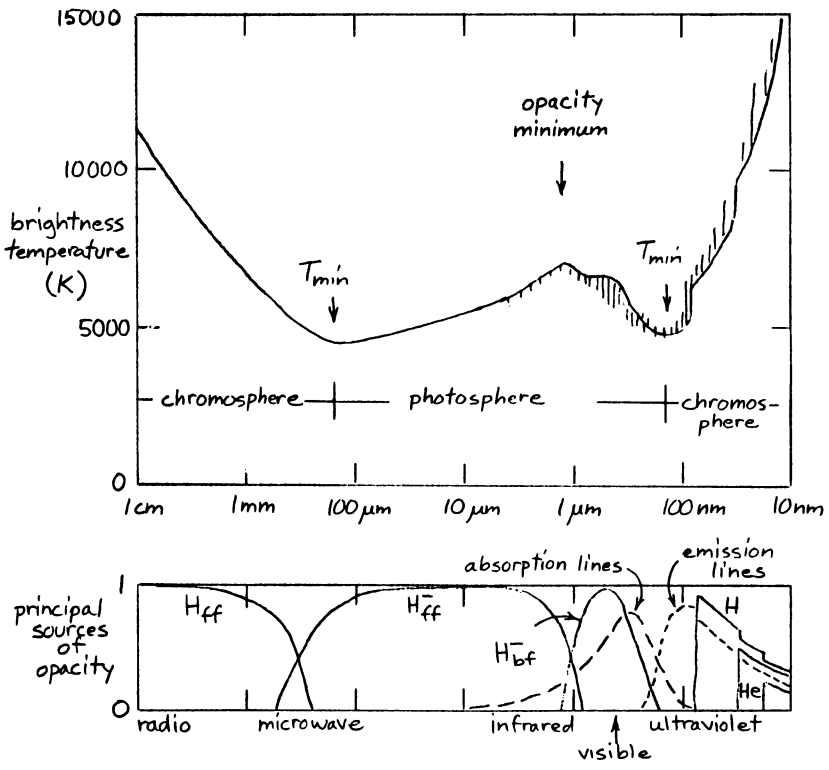

Figure 1. The approximate wavelength distribution of the solar brightness temperature from 1 cm to 10 nm, and the principal sources of opacity at the depths where the emitted radiation is formed.

https://doi.org/10.1017/S0074180900043941 Published online by Cambridge University Press

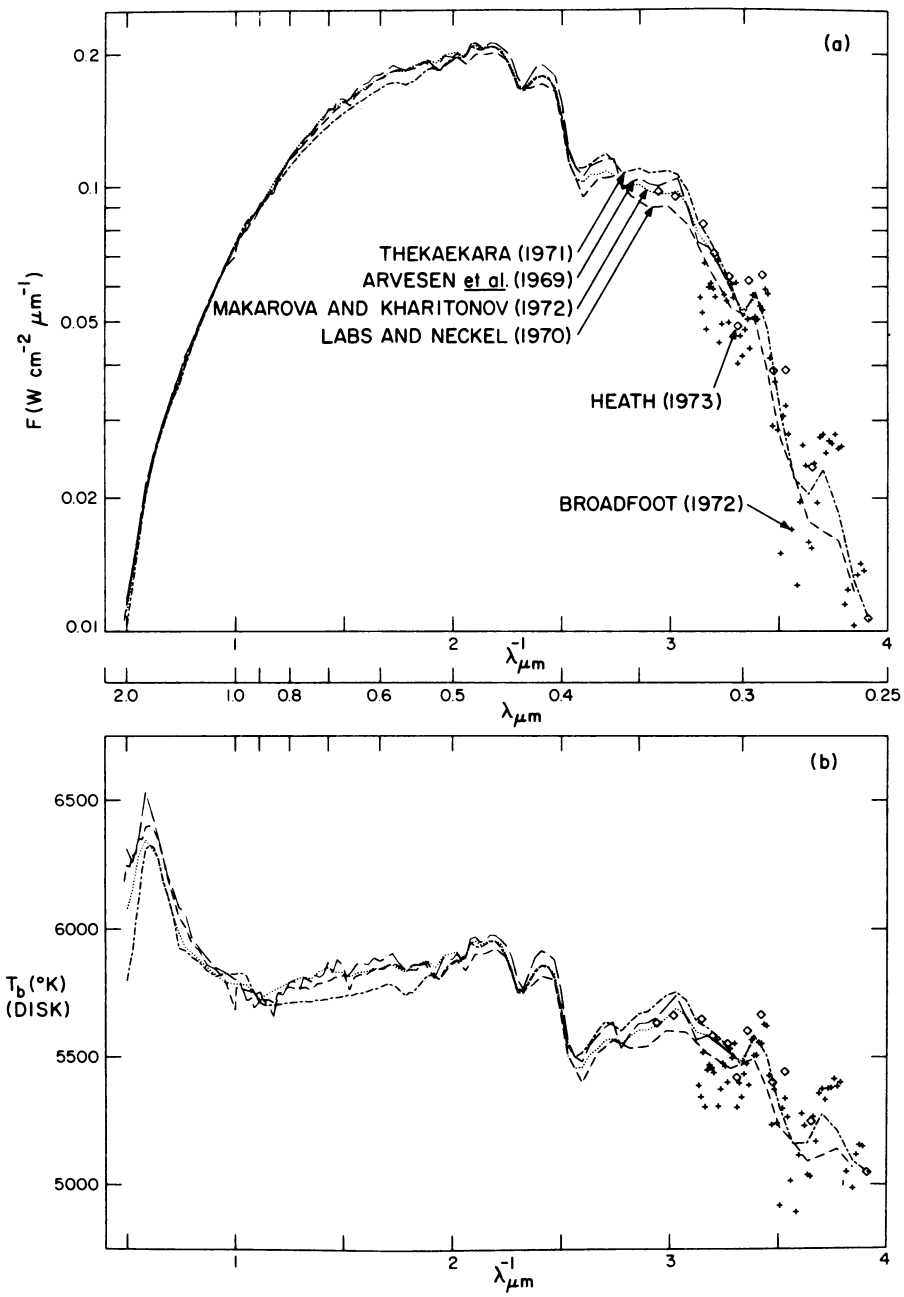

Figure 2. Observed flux in the wavelength range 250 nm - 2 μm (upper panel) and the corresponding disk brightness temperature (lower panel), from Vernazza, Avrett, and Loeser (1976).

https://doi.org/10.1017/S0074180900043941 Published online by Cambridge University Press

Figure 3 shows two types of disk-center intensity distributions in the wavelength range from 1 μm to 200 nm: the mean broad-band distribution and the maximum intensities that occur between absorption lines. The corresponding disk-center brightness temperatures are shown in the lower panel.

The substantial differences between the mean and maximum values are due to the many lines in the spectrum. The observed spectrum in the range 380-420 nm appears in Figure 4. The broad features centered at 393.3 and 396.8 nm in Figure 4 are the K and H resonance lines of Ca II. For $\lambda > 400$ nm the maximum values follow the continuum distribution that would occur with zero line opacities, but for shorter wavelengths such a continuum is not as clearly defined from the observations. When we integrate over wavelength at each depth in the atmosphere to calculate photoionization rates and radiative cooling rates, it is important to accurately account for the many lines in the spectrum, such as those in Figure 4.

Figure 5 shows the continuation of Figure 3 from 200 to 125 nm. The observed central brightness temperature between spectral lines has a minimum of about 4400 K between 160 and 170 nm. The lines in the spectrum change from absorption lines in the range $\lambda > 200$ nm to emission lines in the range $\lambda < 170$ nm.

3. Atmospheric Models

In order to interpret the observed spectrum, we need a model that describes the temperature, density, and other atmospheric parameters as functions of depth. Also, we need to be able to calculate the spectrum from a given set of atmospheric parameters. If we can compute a spectrum that is in good agreement with observations, then the model should provide a description of the actual conditions in the atmosphere. The number of model parameters to be determined is generally much smaller than the number of features to be matched in the observed spectrum (*cf.* Figure 4), so that our confidence in the model increases in proportion to the agreement between computed and observed spectra.

There are two main types of model solar atmospheres: theoretical models and semiempirical models, which differ according to the way the temperature distribution is obtained. In the first case the temperature distribution is calculated according to physical theory with only a few basic parameters chosen to match properties of the solar atmosphere. In the second case the temperature distribution is adjusted by trial and error until the computed spectrum best agrees with observations.

A theoretical one-dimensional model in radiative and hydrostatic equilibrium is characterized by three basic parameters: the solar effective temperature which gives the total flux of energy passing through the atmosphere, the surface gravity, and the relative elemental abundances. Standard values of the first two parameters (from Allen 1973) are $T_{eff} = 5770$ K and $g = 2.740 \times 10^4$ cm s^{-2}. The best solar abundances are those given recently by Anders and Grevesse (1989).

Given such parameters, the goal of the modeler is to develop a computational procedure that includes all the essential physical effects that give rise to the observed spectrum. This is a major ongoing research effort. The most recent theoretical models of the solar photosphere are those of Kurucz (1979) and Anderson (1989).

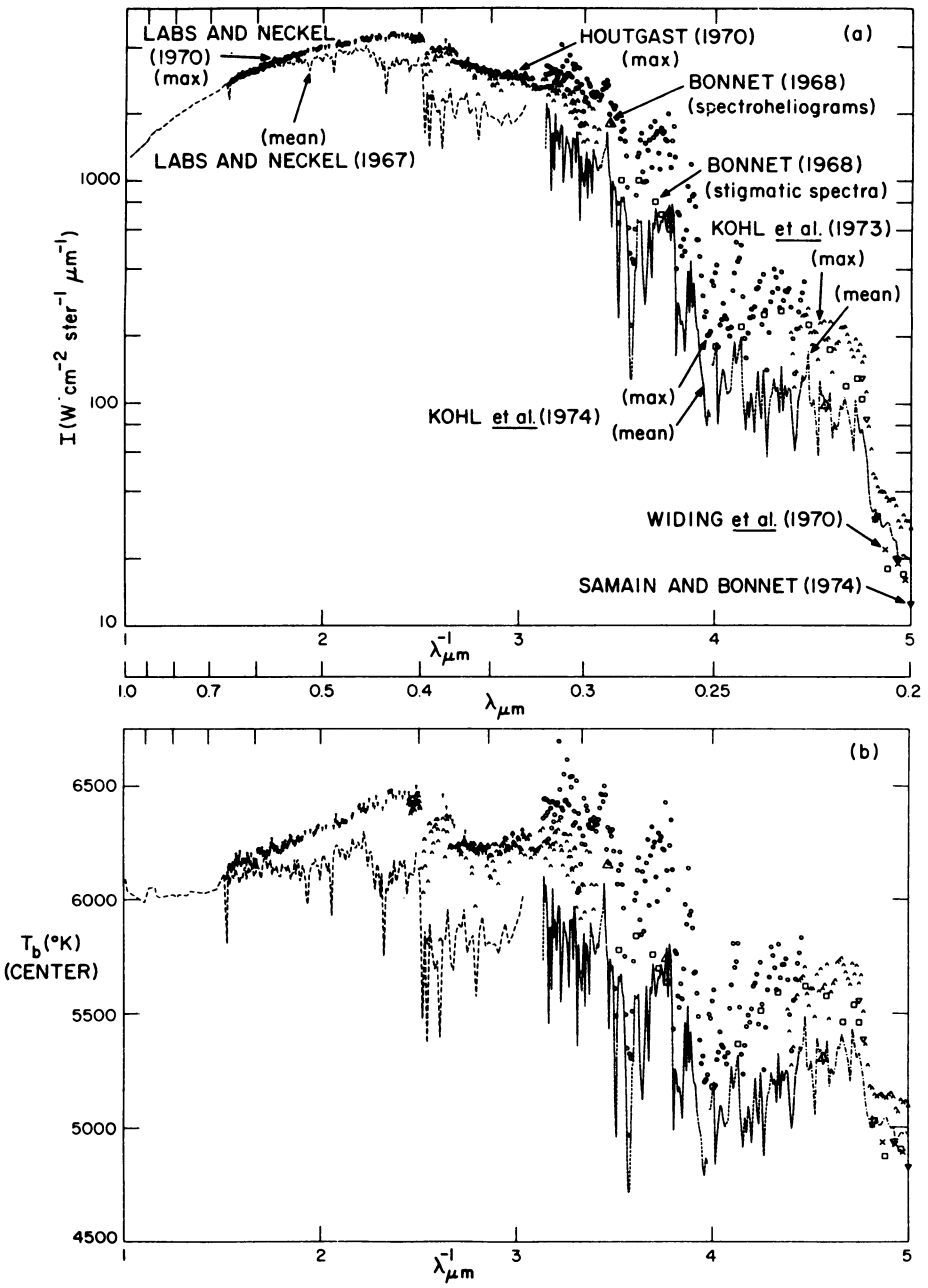

Figure 3. Central-intensity observations in the wavelength range 200 nm - 1 μ (upper panel) and the corresponding central brightness temperature values (lower panel), from Vernazza, Avrett, and Loeser (1976).

https://doi.org/10.1017/S0074180900043941 Published online by Cambridge University Press

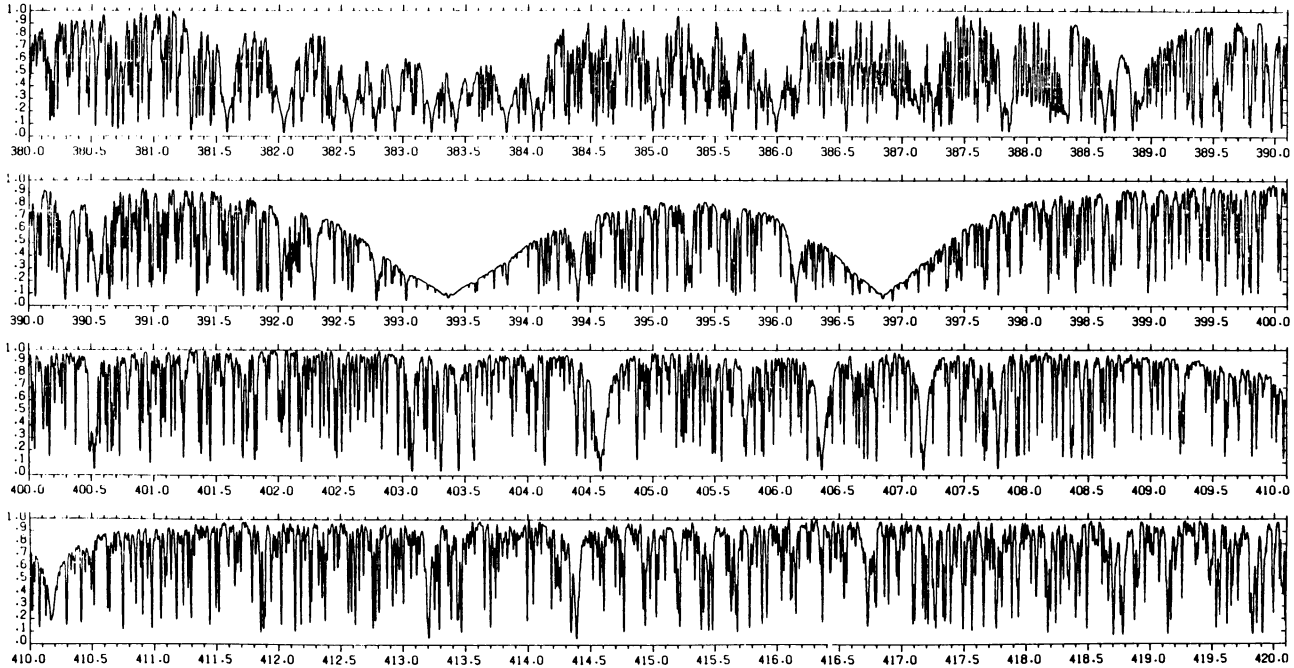

Figure 4. The solar flux between 380 and 420 nm, including the Ca II K and H profiles at 393.3 and 396.8 nm, from Kurucz, Furenlid, Brault, and Testerman (1984). The flux is plotted vs. wavelength in nm on a linear scale between zero and a pseudo-continuum level fitted to the observed flux maxima at 378 and 402 nm.

https://doi.org/10.1017/S0074180900043941 Published online by Cambridge University Press

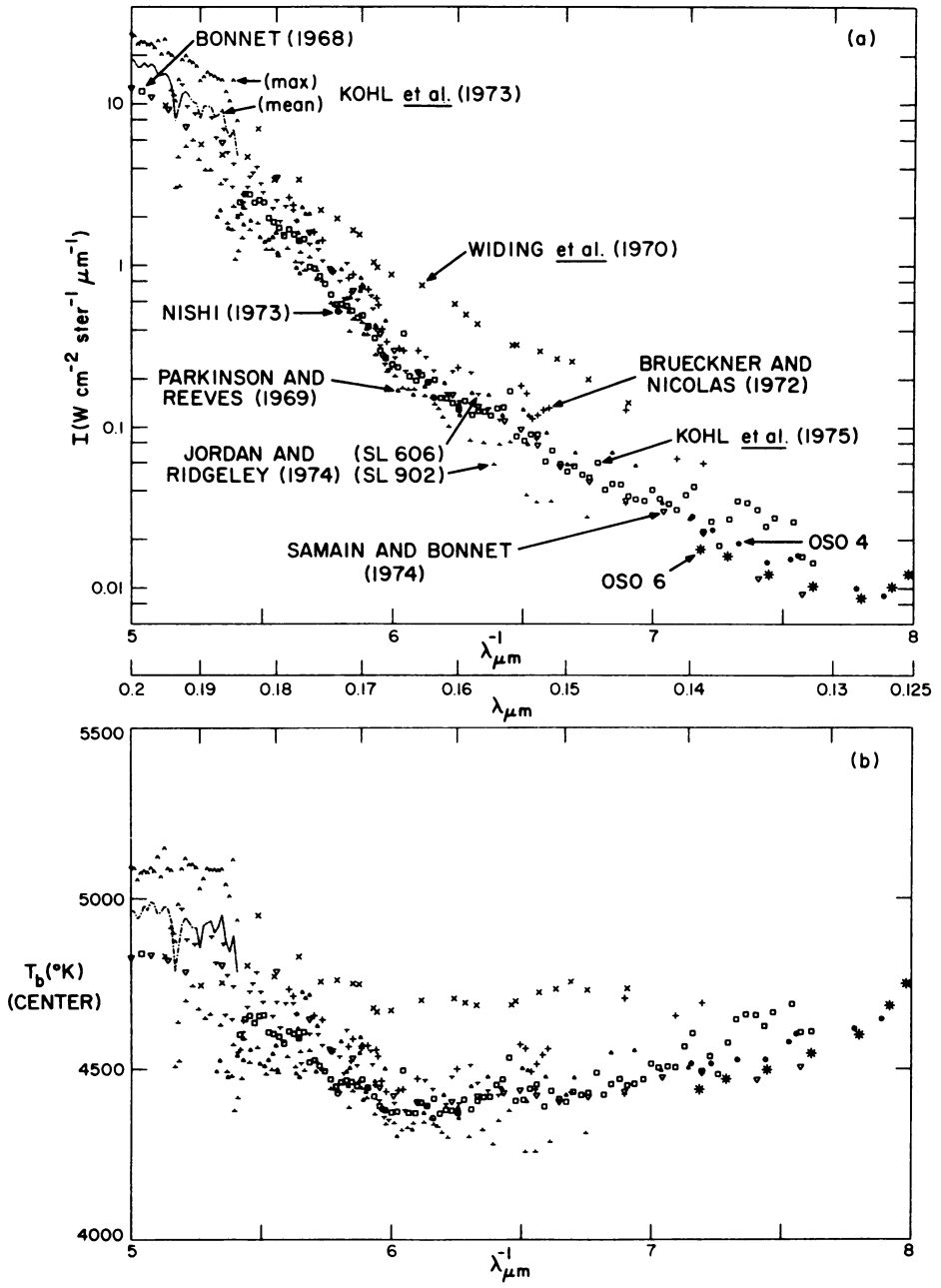

Figure 5. Central-intensity observations in the wavelength range 125-200 nm (upper panel) and the corresponding central brightness temperature values (lower panel), from Vernazza, Avrett, and Loeser (1976).

https://doi.org/10.1017/S0074180900043941 Published online by Cambridge University Press

Both of these models attempt to include the effects caused by millions of atomic and molecular lines in the spectrum. Kurucz adopts the simplifying assumption of LTE (local thermodynamic equilibrium), while Anderson treats the lines throughout the spectrum by a non-LTE statistical method.

Kurucz provides a grid of LTE model atmospheres for effective temperatures between 5500 K and 50,000 K, for gravities from the main sequence down to the radiation pressure limit, and for solar, 1/10 solar, and 1/100 solar abundances. The models were computed with a statistical distribution-function representation of the opacity of almost 10^6 atomic and molecular lines. Kurucz includes convective energy transport using a mixing length theory (see Mihalas 1978, p. 187) in which the mixing length is assumed to be 2 times the pressure scale height.

Anderson also includes a very large number of line transitions, but rather than assuming LTE, he assigns non-LTE effects to lines throughout the spectrum based on a solution of the combined statistical equilibrium and radiative transfer equations for Fe II. The models given by Anderson do not include convective energy transport.

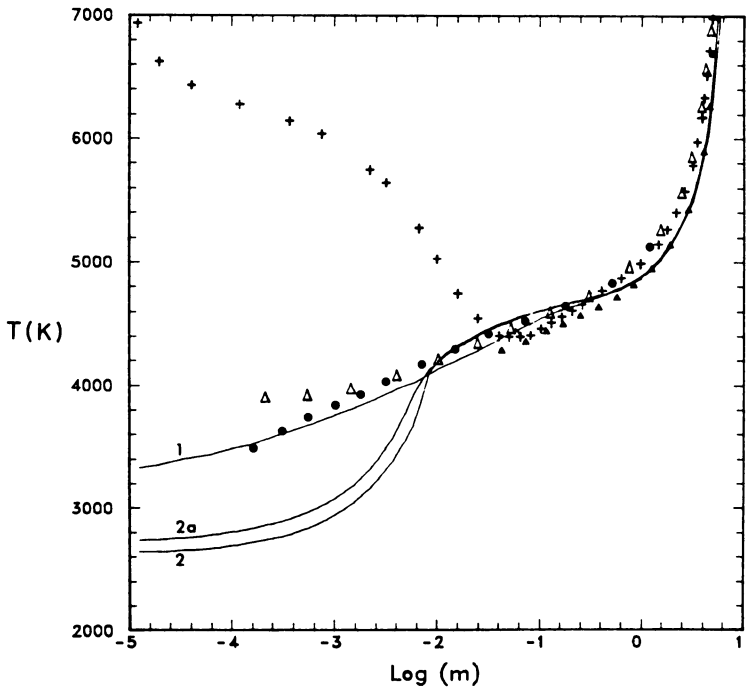

Figure 6. Temperature distributions for the theoretical models of Anderson (1989) and Kurucz (1979) compared with three semiempirical temperature distributions. *Curve 1*: Anderson's LTE theoretical (radiative equilibrium) model. *Curves 2 and 2a*: Anderson's non-LTE theoretical models. *Filled triangles*: Kurucz's LTE theoretical model. *Open triangles*: The LTE semiempirical model of Holweger and Müller (1974). *Plus signs*: The non-LTE semiempirical model of Maltby *et al.* (1986). *Filled circles*: The LTE semiempirical model of Ayres and Testerman (1981) based on carbon monoxide lines.

https://doi.org/10.1017/S0074180900043941 Published online by Cambridge University Press

Figure 6 shows the temperature as a function of the column mass m(g cm^{-2}) for the theoretical models of Anderson and Kurucz compared with three semiempirical temperature distributions (discussed below).

The filled triangles indicate Kurucz's LTE solar model. The curve labeled 1 is Anderson's LTE model. Anderson and Kurucz use different approximations for the line opacities, and they adopt slightly different abundances, which may account for the small differences that occur near log m = -1.

The curve labeled 2 is Anderson's non-LTE model. (His model 2a is the same except that the metallic L $\rightarrow$ L transitions and the molecular transitions are in LTE.) We refer the reader to Anderson's paper for a detailed discussion of his non-LTE theoretical models.

We now consider the semiempirical models shown in Figure 6. The temperature distribution designated by plus signs in this figure is the model given by Maltby *et al.* (1986), which is an improved version of an earlier model by Vernazza, Avrett, and Loeser (1981). In this case the temperature distribution has not been determined theoretically from the constraint of radiative equilibrium, but has been adjusted to match observations. Otherwise, the semiempirical and theoretical models are calculated in similar ways.

Figure 1 showed that the observed brightness temperature increases for $\lambda > 150$ μm and for $\lambda < 160$ nm. The chromospheric temperature rise for log m < -1.4 in the Maltby *et al.* semiempirical model accounts for the brightness temperature rise in these high-opacity wavelength ranges. This model is based on detailed non-LTE calculations for the principal bround-free continua and for representative strong lines. Scattering is assumed for weak lines to simulate non-LTE effects in the chromospheric layers.

The Holweger and Müller (1974) model shown in Figure 6 (open triangles) is an updated version of the earlier LTE model of Holweger (1967), based on a fit to the observed equivalent widths of 900 selected lines, and on central-intensity and center-to-limb observations throughout the visible specturm. This model shows no chromospheric temperature rise because the lines were assumed to be formed in LTE (LTE line opacities, and each line source function S assumed equal to the Planck function B), and because the analysis was based on absorption lines that did not show evidence of a chromospheric temperature rise. Thus the analysis did not include the strong resonance lines. However, lines were included such as Mg I λ5173 for which the central intensities are known to depart from LTE (*cf.* Mauas, Avrett, and Loeser 1988). Since this model is consistent with an extensive and reliable data set, the temperature decrease shown in Figure 6 for log m < -1.4 suggests that this is a decrease not of the kinetic temperature but of a line excitation temperature that is similar for all the lines used in the analysis. Thus, within the limits of uncertainty in central intensity measurements, one can match observations 1) without a chromospheric temperature increase, assuming "incorrectly" that S = B, or 2) with a temperature increase, assuming "correctly" that S decreases relative to B with decreasing gas density.

The semiempirical model of Ayres and Testerman (1981), shown in Figure 6 (filled circles), is based on observations of the fundamental and first overtone bands of carbon monoxide. They find that close to the limb ($\mu = 0.1$) the strongest CO lines in the fundamental band (4.3 to 7.5 μm) have central brightness temperatures as low as 3700 K, and that if these lines are formed in LTE, the temperature decreases monotonically as indicated in Figure 6 with no chromospheric increase. Ayres and Wiedemann (1989) have carried out a detailed study of non-LTE effects in the CO fundamental lines. They find negligible departures from LTE for these lines and conclude that the low line-center brightness temperatures observed near the limb can-

https://doi.org/10.1017/S0074180900043941 Published online by Cambridge University Press

not be explained by non-LTE scattering effects, but must indicate the presence of kinetic temperatures as low as 3700 K. Since other observations clearly indicate that the temperature has a chromospheric rise, such as shown by the crosses in Figure 6, the chromospheric rise evidently does not occur everywhere on the solar surface. Sufficient cool material must be present to account for the low brightness temperatures seen in these CO lines close to the limb.

Above the temperature minimum region in Figure 6 there is a rough agreement between 1) Anderson's LTE theoretical model (curve 1), 2) the LTE semiempirical model based on lines that should be partly affected by non-LTE scattering (open triangles), and 3) the LTE semiempirical model based on the CO lines (filled circles). This agreement may be only fortuitous since a) the non-LTE theoretical model (curve 2) should be a better representation of the radiative-equilibrium atmosphere, without mechanical heating, than the LTE theoretical model, and b) above the temperature minimum region, the non-LTE semiempirical model should be a better representation of the observed atmosphere, with chromospheric heating, than the corresponding LTE model.

Further discussion of the chromosphere is inappropriate in this review of photospheric models. The reader should consult a recent paper by Anderson and Athay (1989) to see the results of adding mechanical heating in the non-LTE theoretical model calculations to produce a chromospheric temperature rise in approximate agreement with the non-LTE semiempirical model in Figure 6.

4. The Temperature Minimum

The Maltby *et al.* (1986) model in Figure 6 can be considered the most recent non-LTE semiempirical model in a sequence starting with the Utrecht Reference Model of the Photosphere and Low Chromosphere (Heintze, Hubenet, and de Jager 1964). The 1964-1986 lineage is indicated in Table 1. This table also gives the minimum temperature adopted for each model.

Table 1

Reference	T_{min} (K)
Heintze, Hubenet, and de Jager (1964)	4500
Gingerich and de Jager (1968)	4600
Gingerich, Noyes, Kalkofen, and Cuny (1971)	4170
Vernazza, Avrett, and Loeser (1973)	4100
Vernazza, Avrett, and Loeser (1976)	4150
Vernazza, Avrett, and Loeser (1981)	4170
Avrett, Kurucz, and Loeser (1984); Avrett (1985); Maltby, Avrett, Carlsson, Kjeldseth-Moe, Kurucz, and Loeser (1986)	4400

https://doi.org/10.1017/S0074180900043941 Published online by Cambridge University Press

The Utrecht reference model was an improved version of an earlier photospheric model of Hubenet (1960). The temperature minimum value of 4500 K in this model was derived by de Jager (1963) from an investigation of the ultraviolet continuum and line spectrum. The model has a chromospheric temperature gradient obtained from eclipse observations by Heintze (1965).

In 1967 an international meeting was held at the Bilderberg Hotel near Arnhem, Netherlands, to establish a new reference model of the solar photosphere and low chromosphere. The papers from this meeting appear in *Solar Physics*, Vol. 3, No. 1, 1968, and are reprinted as a book (de Jager 1968). Agreement was reached on a model, called the Bilderberg Continuum Atmosphere (BCA), representing the continuum observations available at that time (Gingerich and de Jager 1968). The value of T_{min} = 4600K for this model was based on 1) the color temperature at 1600Å observed by Tousey (1963) and his colleagues, and 2) the analysis of the UV carbon monoxide spectrum by Rich (1966) who concluded that $T_{min} = 4500 \pm 100$K.

At this meeting, Athay and Skumanich (1968) argued that $T_{min} \leq 4200$ K, based on studies of the Ca II H and K lines. Later work showed that their analysis underestimated T_{min} for two basic reasons. First, they used observed H and K profiles from Goldberg, Mohler, and Müller (1959) that indicated a minimum K_1 radiation temperature of 4200 K. (K_1 is the intensity minimum in the wing of the Ca II K line just outside the peak that occurs near line center. The K_1 brightness temperature is approximately the temperature minimum value. See Noyes and Avrett 1987.) More recent measurements have shown that this value is closer to 4400 K. Second, they assumed that the lines were formed according to the theory of complete frequency redistribution, which led them to choose $T_{min} \sim 4000$ K to obtain a minimum K_1 brightness temperature of 4200 K. As discussed below, it was realized five years later that the near wings of the H and K lines must be treated according to the theory of partial frequency redistribution, for which these two temperatures are roughly the same.

An improved version of the BCA model, called the Harvard-Smithsonian Reference Atmosphere (HSRA), was proposed by Gingerich *et al.* (1971) based on a variety of new photospheric and chromospheric observations. The minimum temperature was lowered from the BCA value of 4600 K to 4170 K for the following reasons. 1) New rocket observations of the 1650 Å region by Parkinson and Reeves (1969) indicated a minimum brightness temperature of 4400 K or smaller, compared with the 4600 K minimum value used for the BCA. 2) Cuny (1971) carried out a detailed study of how departures from LTE affect the continuum spectrum in the 1520-1680 Å region, and found that silicon and other neutral atoms are underpopulated relative to LTE in the temperature minimum region so that the minimum temperature should be lower, by perhaps 200 K, than the minimum observed brightness temperature. 3) Eddy, Lena, and MacQueen (1969) reported a value of about 4300 K for the brightness temperature at 300 μm. To obtain such a value from the model calculations, T_{min} needed to be in the range 4100-4200 K.

Vernazza, Avrett, and Loeser (1973, 1976, 1981) carried out more extensive non-LTE model calculations, incorporated further observational data, and extended the HSRA model into the chromosphere-coronal transition region. Only minor adjustments for T_{min} were made, since there were no changes in the ultraviolet continuum data used to define the minimum temperature in these models.

During the mid 1970s, however, it became clear that the Ca II and Mg II resonance lines imply higher values of T_{min}. As reviewed by Linsky (1985), the importance of partial frequency redistribution in the wings of the Ca II H and K lines was first recognized at IAU Colloquium No. 19 on Stellar Chromospheres (Jordan and Avrett 1973). Milkey and Mihalas

(1974) studied partial redistribution effects in the Mg II h and k wings and concluded that $T_{min} \geq 4400$ K. Shine, Milkey, and Mihalas (1975) carried out a similar study of the Ca II H and K lines and found that the shape and center-to-limb variation of the computed profiles matched observations much better than the profiles obtained with complete redistribution, and that they could match the absolute K_1 intensity derived from the observations of White and Suemoto (1968) with a minimum temperature of about 4450 K. Ayres and Linsky (1976) carried out a partial redistribution analysis of the Ca II profiles observed by Brault and Testerman (1972) and the Mg II profiles of Kohl and Parkinson (1976). They found $T_{min} = 4450 \pm 130$ K from the Ca II lines and $T_{min} = 4500$ (+80, -110) K from the lines of Mg II.

In 1978 the minimum brightness temperature in the far infrared was found to be higher than the value reported by Eddy, Lena, and MacQueen and others in 1969 (see the review by Mankin 1977). Rast, Kneubühl, and Müller (1978) determined that the minimum brightness temperature is 4530 (+100,-150) K near 130 μm.

As pointed out by Vernazza, Avrett, and Loeser (1981), comparison with the ultraviolet center-to-limb observations of Samain (1980) shows that at wavelengths where the continuum intensity originates on the photospheric side of the temperature minimum the average quiet-Sun model with $T_{min} = 4170$ K predicts less limb darkening than observed, while at wavelengths where the continuum intensity originates on the chromospheric side, less limb brightening than observed. Thus, the computed continuum source function is too flat on both sides of the temperature minimum. At these wavelengths the computed non-LTE continuum source function S is only loosely coupled to the Planck function B, and is much flatter than B in the minimum region. Figure 7 shows the variations of S and B with height h (km) at $\lambda = 160.5$ nm from model C of Vernazza, Avrett, and Loeser (1981). The computed intensities at disk center ($\mu = 1$) and near the limb ($\mu = 0.3$) are indicated in Figure 7 by I (1.0) and I (0.3), respectively.

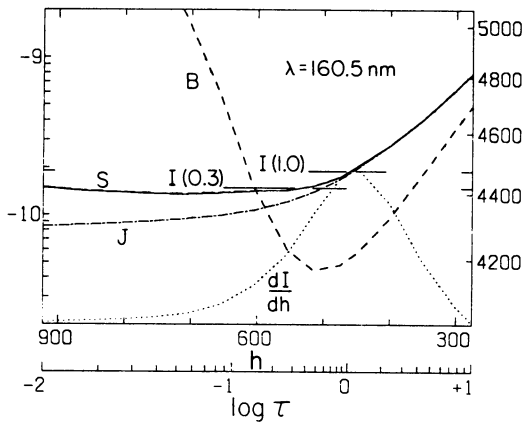

Figure 7. The Planck function B, the continuum source function S, the mean intensity J, and the contribution per unit height dI/dh to the emergent intensity at $\mu = 1$, plotted as functions of height and the continuum optical depth, all at $\lambda = 160.5$ nm. The computed values of I(1.0) and I(0.3), the emergent intensities at $\mu = 1.0$ and 0.3, are indicated. The units for B, S, J, and I on the left are ergs cm^{-2} s^{-1} sr^{-1} Hz^{-1}. The corresponding brightness temperature scale (in K) is given on the right. From Vernazza, Avrett, and Loeser (1981).

https://doi.org/10.1017/S0074180900043941 Published online by Cambridge University Press

These computed intensities are in approximate agreement with observations. If S were closer to B near log τ = 0, we would have to increase T_{min} to keep the computed intensities the same. Neutral silicon and iron are the main contributors to the bound-free absorption and emission near 1600 Å. Thus it is important to examine the accuracy of the computed departures from LTE in Si I and Fe I.

A major uncertainty in the calculations is how to deal properly with the many lines throughout the spectrum. The lines are important 1) in calculating the photoionization-rate integrals that affect the ionization equilibrium of Si, Fe, Mg, C, Al, and other atoms, and 2) in calculating the spectrum for direct comparison with observations. The 1981 model calculations were repeated by Avrett, Kurucz, and Loeser (1984) using the line opacity tables available from R. Kurucz that included more than 1.7 x 10^7 atomic and molecular lines. The various photoionization rates were recomputed using the total line opacity (as a function of temperature and pressure) sampled at 7,000 wavelengths between 1490 and 6050 Å. See Avrett (1985) for further details. They found as a result that the ionization equilibrium of Si, Fe, and Mg in the temperature-minimum region is much closer to LTE than before, e.g., the level-1 Si I departure coefficient at h = 500 km changed from 0.3 to 0.8. In the new calculations that include the spectral lines more realistically, the silicon continuum source function at h = 500 km and $\lambda \sim$ 1600 Å is only about 30% larger than the Planck function, vs. 3 to 4 times larger in the Vernazza *et al.* calculations, and in the similar earlier calculations by Cuny (1971).

Consequently, T_{min} had to be raised from 4170 to 4400 K to maintain agreement between the computed and observed ultraviolet intensities. This modified version of the average quiet-Sun model of Vernazza, Avrett, and Loeser (1981) is tabulated in Appendix A of Maltby *et al.* (1986). (As discussed in the next section, the model given by Maltby *et al.* also has been adjusted in the deepest layers to match available observations as well as possible.)

The 4400 K minimum temperature is consistent 1) with the 130 μm observations of Rast, Kneubühl, and Müller (1978) and subsequent observations by Degiacomi, Kneubühl, and Huguenin (1985) at 50, 80, and 200 μ, 2) with observations in the ultraviolet minimum region (see Cook, Brueckner, and Bartoe 1983; Foing and Bonnet 1984), and 3) with Ca II and Mg II line observations (see Avrett 1985 for a comparison with the H line profiles observed with high spatial resolution by Cram and Dame 1983). As pointed out by Rutten (1988) in a recent review of the non-LTE formation of iron lines in the solar photosphere, the Maltby *et al.* non-LTE semiempirical model finally agreed with the Holweger and Muller (1974) LTE semiempirical model (except for the chromospheric temperature rise) after it was found that some of the earlier non-LTE effects arose artificially in the computer modeling rather than in the Sun.

The only observations that are clearly inconsistent with the Maltby *et al.* model, in the upper photosphere-low chromosphere region, are the central brightness temperature values of 3700 K deduced from the carbon monoxide lines observed near the limb by Ayres and Testerman (1981). These lines were observed earlier by Noyes and Hall (1972) who found a strong 5-minute oscillation of the CO central intensities near disk center which they suggested might be due to adiabatic cooling associated with the oscillation. The same effect could be due to expansion cooling of rising granules as suggested by Nordlund (1985). This work is discussed briefly in Section 7.

It should be noted that in Figure 6 the non-LTE semiempirical temperatures (plus signs) lie below the non-LTE radiative equilibrium temperatures (curve 2) in the minimum region -1.5 < log m < -0.5, and lie above the radiative equilibrium values deeper in the photosphere (log m > -0.5). This means that the flux derivative or net radiative cooling rate

https://doi.org/10.1017/S0074180900043941 Published online by Cambridge University Press

$$\Phi = 4\pi \int \kappa_\nu \, (S_\nu - J_\nu) \, d\nu \quad (\text{ergs cm}^3 \text{ s}^{-1})$$

calculated for the semiempirical model is negative in the minimum region and positive deeper in the photosphere. ($\Phi = 0$ for the radiative equilibrium model.)

In the chromosphere Φ is also positive, and corresponds to the mechanical heating in ergs cm^{-3} s^{-1} responsible for the chromospheric temperature rise. Since the gas density is so much greater in the photosphere than in the chromosphere, small photospheric departures from radiative equilibrium can cause Φ to be numerically larger in the photosphere than in the chromosphere where radiative equilibrium no longer applies. Results given by Avrett (1985) show that the absolute value of $\int\Phi_{min}$, the integral of Φ over the minimum region, exceeds $\int\Phi_{higher}$, the integral over the chromosphere, transition region, and corona. Thus the amount of mechanical energy extracted from the temperature minimum region is larger than the amount of energy needed to heat the chromosphere and corona. The quantity $\int\Phi_{lower}$ defined as the integral over the region log m > -0.5 has not been evaluated for the Maltby *et al.* model, but it appears to be much larger than $\left| \int \Phi_{min} \right|$. These departures from radiative equilibrium may be the result of either oscillations or convective motions in the atmosphere.

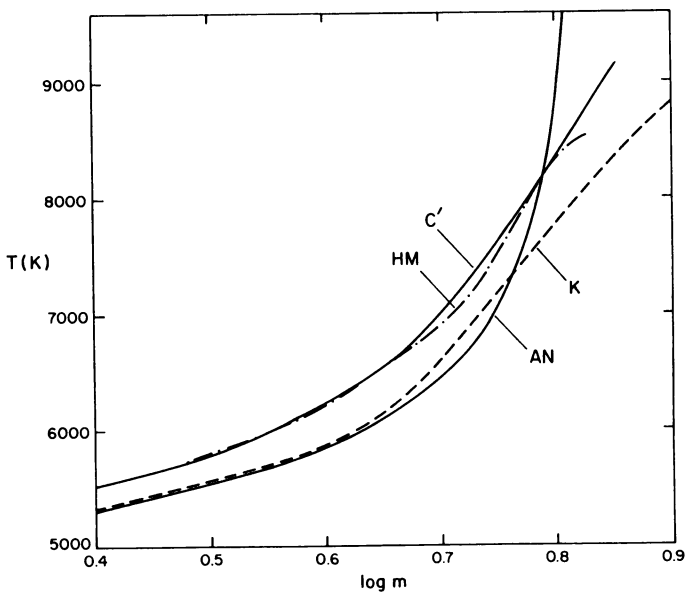

Figure 8. Temperature distributions in the deeper photospheric layers. HM: Holweger and Müller (1974). C′: Maltby *et al.* (1986). AN: Anderson (1989). K: Kurucz (1979).

https://doi.org/10.1017/S0074180900043941 Published online by Cambridge University Press

5. The Deeper Layers

Figure 8 shows a comparison of four temperature models in the deeper part of the photosphere (log m > 0.4). HM is the LTE semiempirical model of Holweger and Muller (1974). C′ is the non-LTE semiempirical model of Maltby *et al.* (1986). At these depths LTE is a good approximation; these two models differ only as the result of a new attempt to calibrate the relative continuum observations of Pierce (1954) in the 1.3-2.5 μm region. See Maltby *et al.*, Appendix A, for details. (Note: this C′ model replaces model C of Vernazza, Avrett, and Loeser 1981.)

AN is the theoretical (i.e., radiative equilibrium) non-LTE model of Anderson (1989) which does not include convective energy transport. K is the theoretical LTE model of Kurucz (1979) which does include convective energy transport using a mixing length theory. Since LTE is a good approximation here, these two models are essentially the same except for the effects of convective transport.

We draw two conclusions from these results. 1) The mixing length approximation adopted by Kurucz (1979) gives a temperature gradient consistent with observations in the deepest layers, and 2) the semiempirical temperature distribution lies 200-500 K above the theoretical temperature distribution.

We stress that these are the properties obtained from average, one-component, static models. It may be that such results are as consistent as can be expected in view of the complex structures and motions that are observed.

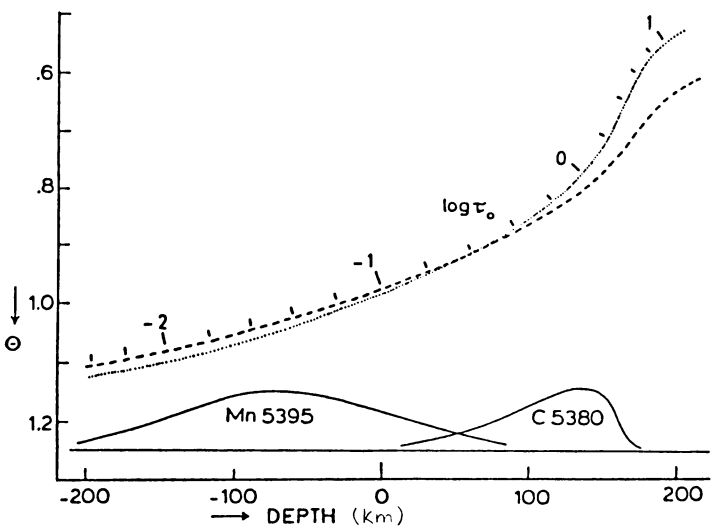

Figure 9. Θ = 5040/T vs. depth in km determined by Elste (1985) for regions with little or no magnetic field (dotted curve) and for plage regions with a magnetic field (dashed curve). τ_0 is the continuum optical depth at 5000 Å.

https://doi.org/10.1017/S0074180900043941 Published online by Cambridge University Press

6. Two-Component Models

Nelson (1978) constructed a two-dimensional model of the photosphere including a physical model of granulation. The temperature distribution was adjusted so that the sum of radiative and convective fluxes remained constant with depth. He concluded that a one-dimensional model which reproduces the observed average intensities and center-to-limb behavior underestimates the temperature gradient in the deep photosphere and overestimates the amount of convective flux penetrating into the visible layers. His mean temperature distribution in the deep photosphere (T > 7000 K) has a steeper gradient than the semiempirical models in Figure 8.

Two recent studies provide insight into the relative photospheric temperature gradients in regions with and without magnetic fields. Elste (1985) derived the temperature gradients at two separate photospheric depths by observing the equivalent widths of the high excitation carbon line at 5380 Å and the ground-level manganese line at 5395 Å. This manganese line also serves as an indicator of longitudinal magnetic fields. Figure 9 indicates the depths at which these two lines are formed and the temperature distributions obtained from regions with little or no magnetic field (dotted curve) and from weak plage regions having a magnetic field (dashed curve). Here $\Theta = 5040/T$. It is well known that plage regions are brighter than quiet regions based on the radiation emitted from the outer photosphere and chromosphere. This work shows that plage regions have flatter temperature gradients in the deep photosphere.

Similar results were found by Foukal, Little, and Mooney (1989) from observations of the deepest observable layers at 1.63 μm. They found that facular flux tubes which are brighter than their surroundings in the visible continuum are darker than surrounding regions at 1.63 μm.

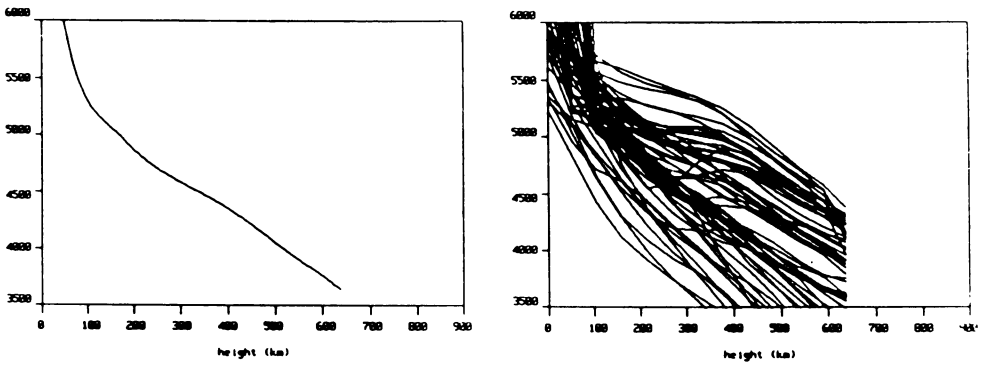

Figure 10. Results from the three-dimensional simulation of Nordlund (1985). *Left*: the horizontally averaged temperature distribution. *Right*: a selection of the individual distributions $T_{x,y}(h)$ that contribute to the average.

https://doi.org/10.1017/S0074180900043941 Published online by Cambridge University Press

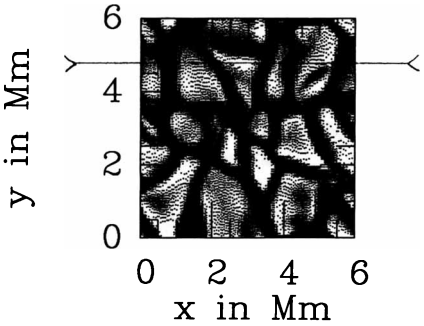

Figure 11. The calculated continuum intensity at 5000 Å in the normal direction as a function of position on the solar surface from one of Nordlund's convection simulations. From A. van Ballegooijen (private communication).

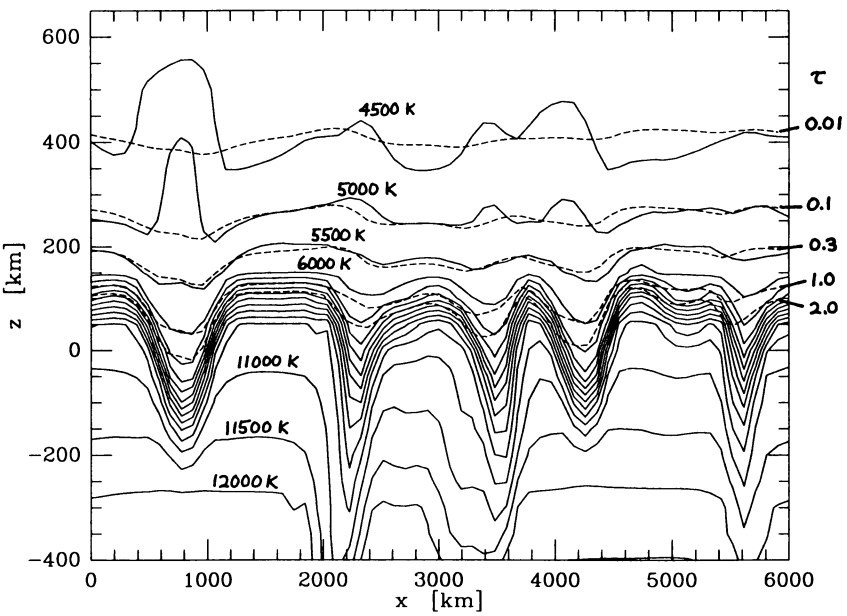

Figure 12. Temperature and optical depth contours in the vertical plane corresponding to the line indicated in Figure 11. From A. van Ballegooijen (private communication).

https://doi.org/10.1017/S0074180900043941 Published online by Cambridge University Press

7. Three-Dimensional Simulations

A comprehensive review of the hydrodynamics of solar granulation was given by Nordlund (1985). (See also his chapter in this volume.) His three-dimensional simulations of granular convection give a very wide range of the calculated temperature as a function of height at different positions x,y on the disk. Figure 10 shows on the right a selection of his calculated $T_{x,y}(h)$ distributions, while the horizontally averaged temperature distribution is shown on the left. This range of values appears to be far beyond the limits of uncertainty indicated by the various semiempirical and theoretical models considered above. The range of temperature distributions appears exaggerated only because all are plotted on a common height scale. Because the H^- opacity is highly sensitive to temperature, the various curves in Figure 10 would appear much closer together if they were plotted on a common optical depth scale.

In the summer of 1988, Nordlund kindly gave this author a detailed tabulation of the results available at that time. Figure 11 and 12 were produced from those results by A. van Ballegooijen (private communicaton).

Figure 11 shows the calculated convective pattern in the visible continuum over a 6000 x 6000 km area near disk center. The horizontal line drawn across the upper part of this figure has been chosen to cross a number of cells and dark lanes. Consider a vertical cut into the atmosphere along this line. Figure 12 is a plot of the temperature contours in this vertical plane. Note that the horizontal scale extends over 6000 km as in Figure 11, but that the height scale ranges over only 1000 km. Temperature contours are given every 500 K between 4500 and 12,000 K. The dark lanes in Figure 11 are clearly apparent in Figure 12 as regions in which low temperatures extend deeply into the atmosphere. On an optical depth scale, however, these depressions are reduced. The dashed lines in Figure 12 are the optical depth contours for τ = 0.01, 0.1, 0.3, 1, and 2 (in the continuum at 5000 Å). Were it not for the tendency for the τ contours to roughly follow the temperature contours, the computed contrast from such structures would be much greater than observed.

Further details of these simulations are given in the chapter by Nordlund in this volume and in a recent paper by Stein and Nordlund (1989).

Further discussion of "The Photosphere as a Radiative Boundary" is given by Anderson and Avrett (1989).

References

Allen, C.W. 1973, *Astrophysical Quantities* (London: Athlone Press).
Anders, E., and Grevesse, N. 1989, *Geochim. Cosmochim. Acta.*, **53**, 197.
Anderson, L.S. 1989, *Astrophys. J.*, **339**, 558.
Anderson, L.S., and Athay, R.G. 1989, *Astrophys. J.*, in press.
Anderson, L. S. and Avrett, E. H. 1989 in *The Solar Interior and Atmosphere*, ed. A.N. Cox, W.C. Livingston, and M. Matthews (Arizona: University of Arizona Press), in press.
Athay, R.G., and Skumanich, A. 1968, *Solar Phys.*, **3**, 181.
Avrett, E.H. 1985, in *Chromospheric Diagnostics and Modelling*, ed. B.W. Lites, (Sunspot, NM: National Solar Observatory), p. 67.
Avrett, E.H., Kurucz, R.L., and Loeser, R. 1984, *Bull. Amer. Astron. Soc.*, **16**, 450.
Ayres, T.R., and Linsky, J.L. 1976, *Astrophys. J.*, **205**, 874.
Ayres, T.R., and Testerman, L. 1981, *Astrophys. J.*, **245**, 1124.

Ayres, T.R., and Wiedemann, G.R. 1989, *Astrophys. J.*, **338**, 1033.
Brault, J., and Testerman, L. 1972, *Preliminary Edition of the Kitt Peak Solar Atlas* (Tucson: Kitt Peak National Observatory).
Cook, J.W., Brueckner, G.E., and Bartoe, J.-D.F. 1983, *Astrophys. J.*, **270**, L89.
Cram, L.E., and Dame, L. 1983, *Astrophys. J.*, **272**, 355.
Cuny, Y. 1971, *Solar Phys.*, **16**, 293.
Degiacomi, C.G., Kneubühl, F.K., and Huguenin, D. 1985, *Astrophys. J.*, **298**, 918.
deJager, C. 1963, *Bull. Astron. Inst. Neth.*, **17**, 209.
deJager, C. 1968, *The Structure of the Quiet Photosphere and the Low Chromosphere* (Dordrecht: Reidel).
Eddy, J.A., Lena, P.J., and MacQueen, R.M. 1969, *Solar Phys*, **10**, 330.
Elste, G. 1985, in *Theoretical Problems in High Resolution Solar Physics*, ed. H.U. Schmidt, Max Planck Institut für Astrophysik, MPA 212, p. 185.
Foing, B., and Bonnet, R.M. 1984, *Astrophys. J.*, **279**, 848.
Foukal, P., Little, R., and Mooney, J. 1989, *Astrophys. J.*, **336**, L33.
Gingerich, O., and deJager, C. 1968, *Solar Phys*, **3**, 5.
Gingerich, O., Noyes, R.W., Kalkofen, W., and Cuny, Y. 1971, *Solar Phys.*, **18**, 347.
Goldberg, L., Mohler, O.C., and Müller, E. 1959, *Astrophys. J.*, **129**, 119.
Heintze, J.R.W. 1965, *Rech. Obs. Astron. Utrecht*, **17** (2).
Heintze, J.R.W., Hubenet, H., and deJager, C. 1964, *Bull. Astron. Inst. Neth.*, **17**, 442.
Holweger, H. 1967, *Zeitz. f. Astrophysik*, **65**, 365.
Holweger, H., and Müller, E.A. 1974, *Solar Phys.*, **39**, 19.
Hubenet, H. 1960, *Rech. Astr. Obs. Utrecht*, **15** (1).
Jordan, S.D., and Avrett, E.H., eds. 1963, *Stellar Chromospheres*, NASA SP-317.
Kohl, J.L., and Parkinson, W.H. 1976, *Astrophys. J.*, **205**, 599.
Kurucz, R.L. 1979, *Astrophys. J. Suppl.*, **40**, 1.
Linsky, J.L. 1985, in *Progress in Stellar Spectral Line Formation Theory*, ed. J.E. Beckman and L. Crivellari (Dordrecht: Reidel), p. 1.
Maltby, P., Avrett, E.H., Carlsson, M., Kjeldseth-Moe, O., Kurucz, R.L., and Loeser, R. 1986, *Astrophys. J.*, **306**, 284.
Mankin, W.G. 1977, in *The Solar Output and Its Variation*, ed. O.R. White (Boulder: Colorado Associated University Press), p. 151.
Mauas, P.J., Avrett, E.H., and Loeser, R. 1988, *Astrophys. J.*, **330**, 1008.
Mihalas, D. 1978, *Stellar Atmospheres*, (San Francisco: Freeman).
Milkey, R.W. and Mihalas, D. 1974, *Astrophys. J.*, **192**, 769.
Nelson, G.D. 1978, *Solar Phys*, **60**, 5.
Nordlund, Å. 1985, in *Theoretical Problems in High Resolution Solar Physics*, ed. H.U. Schmidt, Max Planck Institut fur Astrophysik, MPA 212, p. 1.
Noyes, R.W., and Avrett, E.H. 1987, in *Spectroscopy of Astrophysical Plasmas*, ed. A. Dalgarno and D. Layzer (Cambridge: Cambridge University Press), p. 125.
Noyes, R.W., and Hall, D.N.B. 1972, *Astrophys. J.*, **176**, L89.
Parkinson, W.H., and Reeves, E.M. 1969, *Solar Phys.*, **10**, 342.
Pierce, A.K. 1954, *Astrophys. J.*, **120**, 221.
Rast, J., Kneubühl, F.K., and Müller, E.A. 1978, *Astron. Astrophys.*, **68**, 229.
Rich, J. 1966, *Silicon and Carbon Monoxide Absorption in the Solar Ultraviolet Spectrum*, Thesis, Harvard University, Cambridge, Mass.

Rutten, R.J. 1988, in *Physics of Formation of Fe II Lines Outside LTE*, ed. R. Viotti, A. Vittone, and M. Friedjung (Dordrecht: Reidel), p. 185.
Samain, D. 1980, *Astrophys. J. Suppl.*, **44**, 273.
Shine, R.A., Milkey, R.W., and Mihalas, D. 1975, *Astrophys. J.*, **199**, 724.
Stein, R.F., and Nordlund, Å. 1989, *Astrophys. J. (Lett.)*, in press.
Tousey, R. 1963, *Space Sci. Rev.*, **2**, 3.
Vernazza, J.E., Avrett, E.H., and Loeser, R. 1973, *Astrophys. J.*, **184**, 605.
Vernazza, J.E., Avrett, E.H., and Loeser, R. 1976, *Astrophys. J. Suppl.*, **30**, 1.
Vernazza, J.E., Avrett, E.H., and Loeser, R. 1981, *Astrophys. J. Suppl.*, **45**, 635.
White, O.R., and Suemoto, Z. 1968, *Solar Phys.*, **3**, 523.